Structural response of cold-formed lipped Z purlins – Part 1: Experimental investigation

Meshal Almatrafi[1], Marios Theofanous[1*], Samir Dirar[1], Michaela Gkantou[2]

[1] Department of Civil Engineering, University of Birmingham, Edgbaston B15 2TT, UK

[2] Department of Civil Engineering, Liverpool John Moores University, Liverppol L3 5UG, UK

[*] Corresponding author, Department of Civil Engineering, University of Birmingham, Edgbaston B15 2TT, UK, Email address: m.theofanous@bham.ac.uk

Abstract This paper reports 8 experimental tests on simply supported purlins with lipped Z-sections under gravity loads. The adopted test details are representative of the support conditions typically employed in practice with each specimen comprising two purlins connected to each other at regular intervals with angle struts used in lieu of anti-sag bars and profiled steel sheeting attached to the purlins' top flanges via self-drilling screws. The observed failure modes included primarily distortional buckling and interactive distortional/local buckling. The moment resistance predictions of EN 1993-1-3 and the Direct Strength Method (DSM) were compared against the experimentally obtained moment resistances and it was concluded that the EN 1993-1-3 strength predictions are overly conservative, whilst the DSM offers more accurate strength predictions. The experimental results are utilized in the companion paper where a numerical study on the optimization of the lip size of Z sections is reported.

Keywords: Cold-formed steel, purlins, distortional buckling, local buckling, Z sections, direct strength method

1 INTRODUCTION

Purlins are among the most commonly used cold-formed steel members in construction. They are employed as secondary steelwork to support roof cladding, transfer loads and provide effective restraint to the primary steel members. Typical cross-section shapes adopted as purlins include C-sections, Z-sections and Σ-sections, which may employ lips and intermediate stiffeners of varying complexity to maximise the cross-section stiffness under the intended loading conditions, thus delaying the onset of local and/or distortional buckling and maximising their structural efficiency. Due to their thin-walled nature and complex geometry stemming from their optimized shape, they are prone to a variety of instabilities including local, distortional and lateral torsional buckling as well as interactions thereof as reported in several analytical studies [1-3]. Under gravity loads, purlins can in most cases be assumed to be effectively restrained against lateral torsional buckling, since the attachment of cladding to the top flange usually provides sufficient lateral and torsional restrain to the purlin. However, under uplift conditions, the cladding provides only partial restrain against torsion and lateral torsional buckling tends to govern failure particularly for longer spans. Furthermore, the absence of double symmetry further complicates the structural behaviour of purlins and leads to the development of complicated stress fields [4].

The reduced effectiveness of slender cold-formed steel elements due to local buckling is traditionally accounted for using the effective width concept, originally developed by von Karman [5] as later modified by Winter [6]. The effective width concept relies on the observation that upon local buckling of a slender plate, the compressive stresses are redistributed towards the supported parts of the plate with the central less stiff parts attracting significantly lower stresses. Hence, parts of the constituent plate elements of a cross-section that have been classified as slender are assumed ineffective and only the effective parts are considered in the determination of the cross-section al capacity. This approach is adopted by all international design standards such as North American specifications for cold-formed steel

[7], American Iron and Steel Institute [8], Canadian Standards Association [9] and Eurocode 3 [10, 11]. Although conceptually simple, the application of the effective width method necessitates the determination of effective cross-section properties, which is cumbersome particularly when it needs to be applied iteratively. Treating the cross-section as an assembly of constituent elements without accounting for their interaction has been shown to lead to inaccurate and inconsistent strength predictions for restrained Z and C sections in bending [12], as well as for more traditional cross-section shapes like RHS and I-sections in compression [13]. Furthermore, the adoption of edge stiffeners to improve resistance against local buckling [14] has led to the emergence of distortional buckling in cross-sections subjected to compression [15] or bending [16], an instability mode beyond the scope of the effective width method. Lau and Hancock [17] were the first to derive explicit equations for distortional buckling of lipped channels in compression, which were incorporated in the relevant Australian Standards [11].

Given the increasing complexity of the geometry of modern cold-formed steel sections, the application of the effective width method, originally developed for cross-sections of simple geometry, becomes awkward and its accuracy questionable. Schafer and Pekoz [18, 19] developed the Direct Strength Method (DSM) as an alternative design approach suitable for cross-sections of complex geometry and inherently able to deal with instability modes and their interactions at cross-sectional and member level. The DSM is based on empirical equations relating member strength to its yield stress and its elastic critical buckling stress corresponding to all relevant buckling modes shapes. Key to the application of the DSM is the determination of the elastic critical buckling stress for all relevant buckling mode shapes, which is usually accomplished via the use of software such as the CUFSM [20-22]. Since its original inception and its adoption by American [8] and Australian design standards [9], the DSM has been further

researched extended by several researchers to cover members subjected to bending and shear [23], the effect of perforations [24, 25] and the design of beam-columns [26].

Several researchers have studied the structural behaviour of cold-formed steel purlins experimentally and numerically with the aim of assessing current and developing new design procedures, to verify the structural response under different loading conditions or to develop novel cross-section geometries. Full scale tests on simply supported and continuous purlins employing C- and Z-sections under gravity loads have shown the effect of the location of the deck fasteners with respect to web axis on the response of C-sections [27], with increasing distance of the fastener axis from the purlin web leading to improved structural response. The importance of the spacing of the fasteners on the resulting failure mode and the corresponding failure load was demonstrated experimentally for C- and Z-sections tested in the 4-point bending configuration [13, 28]. It was concluded that effective attachment of a metal deck to the purlins via closely spaced fasteners can suppress the distortional buckling failure mode and even increase the local buckling resistance, whilst the Direct Strength Method (DSM) [18, 19] was shown to be more accurate compared to other design approaches. Design equations for the inelastic lateral torsional buckling strength of C- and Z- purlins under uplift were developed based on full-scale tests [29], whilst tests on the structural response of Σ- purlins attached to a metal deck with a relatively large fixing spacing are reported in [30] under both gravity and uplift loading. In addition to the conventional C-, Z- and Σ- sections, more complex Σ- sections incorporating longitudinal web stiffeners were studied experimentally and numerically [31] and their improved efficiency over conventional Σ- sections as well the ability of the DSM to accurately predict their response was demonstrated. The response of purlins subjected to combined axial force and biaxial bending has also been experimentally and numerically investigated and suitable design equations accounting for the interaction were proposed [32].

Departing from the conventional cold-formed steel C- sections, experimental studies on the global-distortional buckling interaction of stainless steel C- sections have also been reported [33], whilst novel applications such as composite cold-formed steel flooring systems have also been explored and relevant design methods have been developed [34, 35].

This paper reports in detail an experimental study on cold-formed Z-purlins tested under conditions simulating gravity loading. The experimental results are utilized to assess the accuracy of the predictions of European [10, 11] and American design standards [8] and as a benchmark against which numerical models utilized in the optimization of the lip depth of Z sections are validated in the companion paper [36].

2 EXPERIMENTAL PROGRAMME

A series of 8 tests was conducted on Z-section purlins to determine their flexural response. The employed test configuration was designed to simulate the behaviour of simply supported purlins under uniformly distributed loads (UDL) and avoid lateral torsional buckling. The aim of the tests was to obtain fundamental structural performance data to be used for the development and validation of a FE model capable of replicating numerically the experimentally observed structural response as reported in the companion paper [36].

2.1 Material properties

Tensile coupon tests were conducted on material coupons extracted from the mid-width of the flanges of cold-formed sections cut from the same member length as the tested specimens. Three nominally identical coupons were extracted from each section. The applied strain rate during testing was $0.00025s^{-1}$ until the yield stress and $0.0067s^{-1}$ until fracture, in accordance with [37]. Some of the specimens displayed a well-defined yield plateau followed by strain-hardening similar to hot-rolled steels, whilst others exhibited a more rounded material response and an absence of a yield plateau, as shown in Fig.1 where two typical stress-strain responses are depicted. This marked difference in material response of cold-formed steel has been

previously observed by other researchers [28] and increases the uncertainty regarding the appropriate material model to be used in parametric studies. No corner material properties have been obtained and their effect has not been explicitly considered given the small area of the corner regions and the high slenderness of the tested sections, which failed at loads below their elastic moment resistance. Table 1 reports the obtained material properties averaged out for each tested nominal thickness, where t is the measured coupon thickness, E is the Young's modulus, f_y is the yield stress or 0.2% proof stress for coupons not exhibiting a yield plateau, $f_{1.0}$ is the proof stress at 1% plastic strain, f_u is the ultimate tensile stress and ε_f is the strain at fracture. It can be observed that specimens displaying a yield plateau had a higher ductility (i.e. ε_f) compared to the specimens that exhibited a rounded material response. It should be noted that the material yield strength determined from the tests is on average 4.3% higher than the nominal one, which is 450 N/mm^2.

2.2 Specimen geometry

The geometry of the tested sections is representative of the Z-sections commonly used as secondary steelwork supporting roof sheeting in construction. The nominal outer depth h of the sections varies from 175 mm to 300 mm and the nominal thickness t varies from 1.30 mm to 3.00 mm thus encompassing a wide range of non-dimensional distortional and local slenderness. Prior to testing, measurements of the outer flange width b, outer overall depth h, lip depth d and thickness t were taken with a vernier caliper at each specimens' ends and mid-section. The measured section geometry for each section is reported in Table 2, where the average value of measurements of the internal root radius r_i at the flange-web and flange-lip junctions respectively are also reported. It should be noted that average results for top and bottom flange and top and bottom lip are reported since no significant differences in the measured geometry of the top and bottom flange were observed. The section designation starts with the letter Z indicating a Z-section, followed by the nominal section depth and nominal

section thickness. All symbols are defined in Fig. 2. All section dimensions were within 3% percent of their nominal values except Z24630, the flange and lip lengths of which were measured to be 6% larger than the respective nominal values. It should be mentioned that the reported value for the measured thickness t excludes the thickness of the Zinc coating, which was nominally 0.05mm.

2.3 Fabrication and setup

Each specimen consisted of two purlins connected at their top flange by profiled sheeting with the top flanges facing outwards and the bottom flanges facing inwards. The purlins comprising each specimen were attached to each other via angle struts employed in practical applications as anti-sag bars, which were bolted through the specimen webs at 600 mm intervals prior to fixing the sheeting. The distance between the centrelines of the webs of the paired purlins was 250 mm for all specimens, whilst the overall width of the sheeting was 400 mm. In addition to facilitating load application, the sheeting also serves as a means to provide lateral and torsional support to the purlins hence reducing susceptibility to lateral torsional buckling under downward loading. The role of the anti-sag bars in the tests was to provide a connection between the two sections of each specimen at the points of load application and support, hence facilitating a torsional restrain and stabilising the specimen laterally.

Fig. 3 shows a detail of an angle strut employed as anti-sag bar. It should also be mentioned that several purlins were visibly distorted prior to the assembly of the specimens. However, once fastened with the sheeting and the angle struts the global and distortional imperfections of the individual sections reduced significantly. It was observed that the twisting imperfections of the smaller sections were practically eliminated, and the resulting specimens appeared almost perfectly straight, whilst for the larger and stiffer sections, some of the initial twist remained. Given the large scatter typically exhibited by initial geometric imperfections and the effect of

the assembly process on the imperfection patterns and magnitudes it was decided not to measure initial geometric imperfections in the experimental part of the project.

The sheeting was fixed with one self-drilling screw to the middle of the top flange of each purlin every 400 mm. The chosen spacing of 400 mm corresponds to one screw every second trough of the sheeting and lies at the high end of spacing employed in structural applications. An extra pair of fixings was adopted at the end sections over the support, whilst two consecutive pieces of sheeting were screwed to one another at their overlapping crowns. Angle cleats are commonly used to support the purlins on the rafters and provide strengthening against web crippling. Four M12 bolts were used to attach the vertical leg of an angle cleat to the external part of the web of each of the purlins whilst the horizontal leg of the angle was bolted down on a thick plate resembling the flange of a rafter, as shown in Fig. 4 where details of the attachment of the sheeting to the purlins can also be observed. In order to allow free rotation of the purlins at the supports, the plates on which the angle cleats were bolted were placed on top of cylindrical rollers. Similarly, cylindrical rollers were used between the spreader beams and the loading plates.

2.4 Loading and instrumentation

The specimens were tested as simply supported beams with a clear span between the supports of 3000 mm, thus resulting in span-to-depth ratios ranging from 10 to 20.5. An extra 150 mm overhang beyond each support was provided to allow for the ends to move in as the loads are applied; hence the total length of each purlin was 3300 mm. Each specimen was subjected to 4 equal loads applied using two hydraulic actuators and two spreader beams. Each actuator applied a load onto the centre of the spreader beams, which were simply supported at fifth points (600 mm intervals) on the specimens as shown in Fig. 5, where the setup is depicted schematically. This loading arrangement was employed to reflect the loading condition of a

purlin subjected to a uniformly distributed load and to allow significant bending moments to be applied in the presence of low concentrated forces thus ensuring that failure occurs within the constant moment region. The loading points coincided with the location of the angle struts and were hence deemed torsionally restrained, whilst the chosen spacing of 600 mm between loading points results in a constant moment region with a length equal to 20% of the member length which is within the limits set by EN 1993-1-3 [10].

Between the roller support of each spreader beam and the specimen a 20 mm thick and 80 mm wide plate used to facilitate a uniform distribution of stresses below the loading point and avoid local bearing failure. The hydraulic actuators were being lowered at a speed of 1.5 mm/min, thus replicating static loading conditions. In order to eliminate any effect of the loading speed, loading was paused for 2 minutes at 10 kN intervals in the beginning of the test and at 1 kN intervals close to the ultimate load. This is shown as distinct drops in the load-deflection curves in the following section of the paper where the results are reported. Three LVTDs under each purlin were used to monitor the vertical deflections at mid-span and adjacent load points. The LVDT readings were utilised to check whether the two purlins of each specimen exhibited identical load-deflection characteristics and the results are reported in the next section. Additional LVTDs were positioned on either side of the mid-span monitoring the horizontal deflections to determine whether any lateral torsional buckling was occurring during the testing. Moreover, the strain distribution and the resulting curvature of the tested sections were monitored and recorded at mid-span, where the maximum moment occurs. Two strain gauges were affixed on the web of each purlin of each specimen at a distance of 30 mm from the top and bottom flange respectively. Fig. 6 depicts a specimen prior to the initiation of testing where the setup and employed instrumentation including the attached strain gauges and employed LVDTs can be clearly seen.

In past experimental and numerical studies [23, 38] the spacing of the screws attaching the sheeting to the purlins was shown to affect the failure load and failure mode of each specimen if several fixings are provided at closely spaced intervals. This effect is expected to be negligible for the relatively large spacing adopted herein. Therefore it is assumed that neither local nor distortional buckling of the tested sections is restrained by the attached sheeting and all specimens are free to develop both local and distortional buckling without the cladding providing any stiffness that is likely to suppress these buckling modes. This was verified by the observed failure modes which were not seen to be affected by the location of the fixings as will be discussed subsequently.

3 RESULTS AND DISCUSSION

3.1 Moment resistance and failure modes

Table 3 reports key experimental results including the ultimate moment M_u and the observed failure mode. The ultimate moment is determined based on the recorded maximum applied loads, assuming that they are equally distributed between the paired purlins. The elastic moment resistance M_{el}, as determined with measured geometric and material properties, the M_u/M_{el} ratio and the elastic critical buckling moments corresponding to local and distortional buckling, $M_{cr,l}$ and $M_{cr,d}$ respectively, as determined with the aid of the CUFSM software [20], are also reported to facilitate the discussion of the results in section 4. The letters "L" and "D" and "WC" refer to local buckling, distortional buckling and web crippling respectively and correspond to the observed failure modes at or shortly after the attainment of the failure load. In most cases failure occurred at moments below the elastic moment resistance of the cross-section, with only one section reaching or exceeding its elastic moment resistance. For all tests reported herein failure occurred in the constant moment region, whilst, where web crippling is indicated as a failure mode, this relates to the observed localised plastic deformation at the loading point which occurred after the maximum load was attained and is not believed to have triggered failure.

Figs. 7-14 show the failure modes of the tested specimens as captured at, or shortly after the attainment of the failure load. During testing, specimens Z14620 and Z24620 displayed pronounced deformations consistent with distortional buckling in the opening mode within the constant bending moment region (Figs. 8 and 13) as the load was approaching and shortly after the attainment of the ultimate load. Specimens Z14613, Z 17613, Z17625 and Z24615 exhibited a similar response, with the difference being that the distortional buckling mode interacted with local buckling of the compressed lip of the sections, as evidenced in Figs. 7, 9, 10 and 12, whereupon failure occurred. Specimens Z20620 and Z30718 failed by distortional buckling weakly interacting with local buckling of the flange, closely followed by web crippling close to the loading points. It should be noted that the web crippling deformations (i.e. localization of failure under one of the central loading platens as shown in Figs. 11 and 14) occurred after the ultimate load was attained; hence it is believed that web crippling did not affect the moment resistance. Furthermore, specimen Z17625 experienced distortional buckling and localised buckling of the lip after the attainment of its elastic moment resistance.

Overall, the observed failure modes accord well with the elastic critical buckling moments reported in Table 3. As expected, due to the strongly stable post buckling response associated with local buckling compared to distortional buckling, in cases where the $M_{cr,l}$ is significantly larger than $M_{cr,d}$ as is the case for Z14620, distortional buckling is the observed failure mode without any evidence of local buckling. In cases where the elastic critical buckling moments for local and distortional buckling are closer to each other and when the critical local buckling moment is smaller than the critical distortional buckling moment ($M_{cr,l}<M_{cr,l}$), distortional buckling of the compressed flange occurs followed by localisation of plastic deformations in the compressed lip, whereupon a marked drop in strength occurs.

3.2 Load – deformation response

The total applied load and mid-span deflections of the twin purlins comprising each specimen have been utilized to obtain the overall load-deformation response. Figs. 15 a) and b) depict the load-deformation response of specimens Z17613 and Z17625 respectively. Both twin purlins comprising each specimen can be seen to behave very similarly in the initial part of the loading, as their respective curves are almost identical to one another up to failure, whereupon the response diverges. It can be clearly seen that the more slender section Z17613 exhibits an almost perfectly linear response with minimal loss of stiffness prior to failure, which occurs due to interaction between local and distortional buckling. The stockier section Z17625, which fails at a load 6% higher than the load corresponding to its elastic moment resistance, displays a gradual loss of stiffness, as the partial plasticisation of the cross-section causes the curve to exhibit a small plateau when approaching the ultimate load. Both specimens Z14613 and Z14620 behave in a similar way to Z17613 as shown in Fig. 16.

Figs. 17 a) and b) show the load-deformation response of specimens Z24615 and Z24620 respectively. Specimen Z24615, which failed due to interaction between distortional and local buckling, displays a very similar response to that of purlin Z17613, with the twin purlins of the specimen demonstrating identical load-deflection response until the ultimate load is reached. Specimen Z24620, the failure of which involved distortional buckling shows a diverging response between the two purlins, arguably due to the pronounced initial twist imperfection of the purlins which was not eliminated when the specimen was assembled as was the case for the smaller and thinner sections.

Figs. 18 a) and b) depict the load-deformation response of specimens Z20620 and Z30718 respectively. Despite both specimens failed due to distortional buckling and followed by web crippling after the ultimate load was achieved, they show different load-deformation responses.

Specimen Z20620 displays identical response for both purlins, whilst the twin purlins comprising Z30718 are seen to exhibit different stiffness in terms of the recorded load-vertical deflection response at the onset of loading. This is attributed to the pronounced initial twist imperfection of the purlins, which vanished with under increasing load.

Examining the evolution of strains with increasing load offers significant insight on the structural response of the tested specimens. In Fig. 19 the recorded strains on the web of each purlin are plotted against the applied moment at mid-span for specimen Z17613. To facilitate the discussion, the elastic critical buckling moments for local and distortional buckling $M_{cr,l}$ and $M_{cr,d}$, reported in Table 3, are also depicted as a horizontal dotted line and a horizontal solid line respectively. As expected, for both purlins, the strain gauges attached 30 mm below the top flange, denoted as "top", yield negative strain readings, whilst the strain gauges denoted as "bottom", which were affixed on the web at 30 mm above the bottom flange give positive readings. Due to the symmetric arrangement of the twin purlins of each specimen, the strain readings are almost identical for both purlins throughout the applied loading regime even beyond the attainment of the ultimate load. The obtained moment-strain response is initially linear for both the "top" and "bottom" strain gauges with the respective readings of the "top" strain gauges being a mirror image of those of the "bottom" strain gauges. The recorded tensile strains remain linear and elastic (i.e. significantly lower than the yield strain) throughout the loading, whilst a sharp departure from linearity occurs for the compressive strains at about 6.5 kNm, whereupon the compressive strains increase significantly with only a small increase in the applied moment. It should be noted that although the elastic critical buckling moment for local buckling is smaller than that for distortional buckling, the observed failure mode and hence the cross-sectional instability that triggered the sudden increase in compressive strains is

believed to be distortional buckling and not local buckling, since only distortional buckling deformations were observed prior to the attainment of the ultimate load.

Fig. 20 depicts the evolution of strains with increasing load for specimen Z17625, which is the stockiest among tested cross-sections and the only one that exceeded its elastic moment resistance, denoted with a horizontal solid line in Fig. 20. Contrary to the observations made for Z17613, both compressive and tensile stresses exhibit an almost identical behaviour prior to the attainment of the ultimate load, thus verifying that the cross-section remained fully effective until failure. Based on the material properties of Z17625 reported in Table 1, the yield strain was determined equal to 0.0022. Assuming a linear strain distribution throughout the section web, the theoretical strain values at the location of the strain gauges when the elastic moment resistance is reached (i.e. when the strain at the extreme fibre is 0.0022) have been determined equal to 0.0015 and are depicted in Fig. 20 as dotted vertical lines. The theoretical strain values are in perfect agreement with the recorded compressive strains at the "top" strain gauge location and are very close to the values recorded by the "bottom" strain gauges, thus confirming material yielding occurred when M_{el} was reached and that the section exhibited inelastic bending capacity [39]. Hence, the distortional buckling of the compressed flanges and the localised buckling of the lip that were observed during the test occurred after the attainment of the elastic moment resistance and were triggered by material yielding and the resulting loss of stiffness.

Finally, the recorded strains are also utilised to determine the curvature of each purlin of the tested specimens. In Fig. 21, the moment at midspan M, normalized by the elastic moment resistance M_{el}, is plotted against the curvature k, normalised by the curvature corresponding to the elastic moment resistance $k_{el}=M_{el}/EI$, for sections Z17613 and Z17625. The curvature is obtained by dividing the difference in the recorded strain values by the distance between the

strain gauges. For specimen Z17613, both purlins exhibit an identical response which remains perfectly linear until the applied moment reaches 65% of the elastic moment resistance, whereafter distortional buckling occurs and the failure moment is reached. For specimen Z17625 yielding causes a gradual loss of stiffness beginning at approximately 80% of the elastic moment resistance, as shown in Fig. 21 b). These observations are in accordance with the previous discussion on the moment-strain behaviour shown in Figs. 19 and 20. Similar observations were made for the remaining specimens.

It should be noted that the above discussion was based on the results obtained for the single test conducted for each nominal cross-section size considered. Experimental variation in structural testing is to be expected and hence the behaviour of a single specimen may not be representative. To ensure the reliability of the obtained experimental results, the analytically determined stiffness has been compared to the experimentally obtained one and the agreement was observed to be perfect thus verifying the validity of the experimental setup. Deviation from the linear response occurs with the occurrence of buckling, yielding or interactions thereof. The tested material coupons were seen to give very consistent results in terms of Young's modulus and yield strength (or nominal yield strength), hence the scatter of the material response can be said to be minimal and the reported material properties are deemed representative. The main source of potential experimental scatter is the occurrence of local and/or distortional buckling, the occurrence of which strongly depends on the geometric imperfections present in the specimens, which tend to vary significantly among nominally identical structural components. The effect of initial geometric imperfections on the structural response of purlins is studied in detail numerically in the companion paper [36].

4 ASSESSMENT OF DESIGN CODES

In this section the experimentally obtained moment resistances M_u are compared against the design predictions of two international structural design standards, namely EN 1993-1-3 [10] and the Direct Strength Method (DSM) [8].

As discussed in the Introduction, the European design framework [10, 11] for cold-formed steel sections is based on the concept of effective section, according to which the effect of cross-section instabilities on moment resistance is accounted for by assuming that parts of the section are ineffective due to local and/or distortional buckling. The cross-section is treated initially as a collection of plated elements and the plate slenderness of the compressed elements is determined according to Equation (1):

$$\overline{\lambda_p} = \frac{c/t}{28.4\varepsilon\sqrt{k_\sigma}} \quad (1)$$

where k_σ is the buckling factor corresponding to applied stress distribution and element support conditions, c/t is the width to thickness ratio and $\varepsilon = \sqrt{\frac{235}{f_y}}$ is a material parameter accounting for yield strength. If $\overline{\lambda_p}$ is larger than the codified limits, an effective width factor ρ is determined according to the provisions of EN 1993-1-5 [11] and parts of the compressed elements are assumed ineffective. Thereafter, the effect of distortional buckling is considered following the provisions of EN 1993-1-3 [10], according to which the flange with the edge stiffener is treated as a compression element with continuous partial restraint the stiffness of which is defined according to the geometry of the cross-section. The distortional buckling slenderness $\overline{\lambda_d}$ is determined and a reduced flange/stiffener cross-section is considered by considering a reduced thickness t_{red} if $\overline{\lambda_d} > 0.65$. At the end of this lengthy and iterative procedure an effective cross-section emerges the effective section modulus corresponding to a linear stress distribution W_{eff} of which is determined, and the moment resistance is obtained according to Equation (2):

$$M = \frac{W_{eff}\, f_y}{\gamma_{M0}} \quad (2)$$

where W_{eff} is the effective section modulus, f_y is the material yield strength and γ_{M0} is the partial factor for cross-section resistance equal to 1. It should be noted that the European guidance cannot be used to predict the expected failure mode, as the effects of local and distortional buckling are reflected simultaneously in the geometry of the effective section.

Contrary to the European design guidance that treats cross-sections as an assembly of their elements, the DSM treats cross-sections as a whole. The moment resistances to local buckling and distortional buckling, M_{nl} and M_{nd} respectively, are determined separately and the minimum of the two is the moment resistance M_{DSM}. Given that no lateral or torsional deformations of the purlins were observed during testing, restrained bending about the geometrical axis parallel to the flanges of the sections was assumed in the determination of the elastic critical buckling moment using CUFSM, thus reflecting the effect of the employed sheeting and angle struts. Following this approach, the DSM predicts that all specimens would fail by distortional buckling (i.e. $M_{nl}>M_{nd}$), with the exception of specimen Z24615, for which local buckling is predicted. As discussed in Section 3.1, distortional buckling was observed for all specimens, hence the DSM correctly predicts the observed failure mode with the only exception being Z24615, for which M_{nl} is marginally smaller than M_{nd} (M_{nl}=12.79 kNm<M_{nd}=12.82 kNm).

Table 4 reports the design predictions for both methods based on measured geometry and material properties as well as predicted over experimental moment resistance ratios and the relevant non-dimensional slenderness values for distortional and local buckling λ_d and λ_l respectively. Furthermore, the moment resistance predictions of both design methods ($M_{pred.}$) are normalised by the experimental moment resistance (M_u) and plotted against non-

dimensional slenderness values for distortional buckling λ_d in Fig. 22. Overall, both design methods appear to offer reasonably accurate predictions for the tested sections with a mean predicted over experimental moment resistance of 0.87 and 0.95 for EN1993-1-3 [10,11] and DSM [8] respectively and corresponding coefficients of variation of 7% and 9%. In both Table 4 and Fig. 22 it can be seen that both design methods offer very similar predictions for stockier sections λ_d<1.04, whilst with increasing slenderness the DSM predicts higher bending resistances than the EN 1993-1-3 [10, 11], which on average are closer to the experimentally determined moment resistances.

5 CONCLUSIONS AND FURTHER RESEARCH

Eight experimental tests on twin purlins connected to each other with angle struts and cladding have been conducted and the key experimental results were reported in detail. It was observed that the structural response of the more slender (thinner) sections was linear until the attainment of the ultimate load, whereas for the stockier (thicker) sections gradual loss of stiffness due to yielding prior to failure was evident and the response became more curved close to the ultimate load. In general, the load–deflection curves of the twin purlins of the smaller sections (Z14613, Z14620, Z17613, Z17625, Z20620 and Z24615) were in close agreement with each other up to the ultimate load, thus revealing that the load and corresponding deformation was equally shared between the purlins comprising each specimen. However, for the larger and hence stiffer sections (Z24620, Z30718) some discrepancy was observed at the onset of loading. This is attributed to the fact that the struts and sheeting were sufficiently stiff to limit the pronounced twisting imperfections of the slender purlins, whilst this was not the case for the stiffer purlins as discussed in Section 2.2. For all specimens distortional buckling was the prevailing failure mode followed by local buckling of the lip for those sections having similar values of critical buckling stresses for local and distortional buckling. Finally, both the EN1993-1-3 [10,11] and

the DSM [8] were seen to offer conservative and consistent strength predictions, with the DSM predicting on average 8% higher strengths than the EN 1993-1-3 and correctly predicting the experimental failure mode as distortional buckling. The obtained experimental failure modes and load-deformation responses are utilised in the companion paper to validate the developed numerical model [36], which are utilized to optimize the lip size of lipped Z-sections.

ACKNOWLEDGEMENTS

The supply of specimens and financial support from Albion Sections Ltd is very gratefully acknowledged. The authors would also like to thank Mr Thomas Jarvis and Mr Rodrigo Carles for their involvement in the experimental part of the project. The first author would like to thank the Saudi Arabian Cultural Bureau and Umm Al Qura University for sponsoring his doctoral studies.

REFERENCES

[1] Dias Martins A., Landesmann A., Camotim D., Borges Dinis P. Distortional failure of cold formed steel beams under uniform bending: Behaviour, strength and DSM design. Thin-Walled Structures 118, 196-213, 2017.

[2] Basaglia C, Camotim D., Goncalves R., Graca A. GBT-based assessment of the buckling behaviour of cold-formed steel purlins restrained by sheeting. Thin-Walled Structures 72, 217-229, 2013.

[3] Dias Martins A., Camotim D., Goncalves R., Borges Dinis P. GBT-based assessment of the mechanics of distortional-global interaction in thin-walled lipped channel beams. Thin-Walled Structures 124, 32-47, 2018.

[4] Vieira L.C.M., Malite M., Schafer B.W. Simplified models for cross-section stress demands on C-section purlins in uplift. Thin-Walled Structures 48(1), 33-41, 2010.

[5] Von Karman T, Sechler E.E., Donnel LH. The strength of thin plates in compression. Trans ASME, 54(APM 54–5):53, 1932

[6] Winter G. Strength of thin-walled compression flanges. Trans ASME 1,112, 1947.

[7] North American Cold-formed Steel Specification (NAS). North American specification for the design of cold-formed steel structural members, American Iron and Steel Institute, Washington, D.C, 2001.

[8] AISI. North American Specification. Appendix 1: Design of cold-formed steel structural members using the Direct Strength Method. 2004 supplement to the north American specification for the design of cold-formed steel structures, American Iron and Steel Institute, Washington (DC), 2004.

[9] AS/NZS 4600:2005. Cold formed steel structures. Australian/New ZealandStandard, 2005.

[10] CEN. Eurocode 3: Design of steel structures, Part 1.3: General rules-supplementary rules for cold formed members and sheeting. Brussels, European Committee for Standardization, 2005.

[11] CEN. Eurocode 3: Design of steel structures, Part 1.5: Plated structural elements. Brussels, European Committee for Standardization, 2005.

[12] Schafer B.W. and Trestain T.W.J. Interim design rules for flexure in cold-formed steel webs. 16th International Specialty Conference on Cold-Formed Steel Structures, 2002.

[13] Theofanous M. and Gardner L. (2012). Effect of element interaction and material non linearity on the ultimate capacity of stainless steel cross-sections. Steel and Composite Structures 12(1), 73-92.

[14] Desmond T. P., Pekoz T., and Winter G. Edge stiffeners for thin-walled members. Struct. Div., ASCE, 107(2), 329-353, 1981.

[15] Hancock, G. J., Distortional buckling of steel storage rack columns. Journal of Structural Engineering, ASCE. 111(12): 2770-2783, 1985.

[16] Yu C. and Schafer B.W. Distortional buckling tests on cold-formed steel beams. Journal of Structural Engineering 132(4), 515-528, 2006.

[17] Law S.C.W. and Hancock G.J. Distortional Buckling Formulas for Channel Columns. Journal of Structural Engineering 113 (5), 1063-1078, 1987

[18] Schafer, B.W. & Peköz, T. Direct strength prediction of cold-formed steel members using numerical elastic buckling solutions. International Specialty Conference on Cold-Formed Steel Structures: Recent Research and Developments in Cold-Formed Steel Design and Construction, pp. 69, 1998.

[19] Schafer B.W. Review: The Direct Strength Method of cold-formed steel member design. Journal of Constructional Steel Research, 64(7-8), 766-778, 2008.

[20] Li, Z. & Schafer, B.W. Buckling analysis of cold-formed steel members with general boundary conditions using CUFSM: Conventional and constrained finite strip methods", 20th

International Specialty Conference on Cold-Formed Steel Structures – Recent Research and Developments in Cold-Formed Steel Design and Construction, pp. 17. 2010.

[21] Ádány, S. & Schafer, B.W. Buckling mode decomposition of single-branched open cross-section members via finite strip method: Derivation. Thin-Walled Structures 44(5): 563-584, 2006.

[22] Ádány, S. & Schafer, B.W. Buckling mode decomposition of single-branched open cross-section members via finite strip method: Application and examples. Thin-Walled Structures 44(5): 585-600, 2006.

[23] Pham C.H. and Hancock G.J. Direct strength design of cold-formed purlins. Journal of structural engineering, 135(3), pp.229-238, 2009.

[24] Moen CD. Schafer BW. Stability of cold-formed steel columns with holes. In: Proceedings of the international colloquium on stability and ductility of steel structures. 2006.

[25] Moen C.D. and Schafer B.W. Direct strength method for design of cold-formed steel columns with holes. Journal of Structural Engineering (ASCE), 137 (5): 559-570, 2011.

[26] Schafer B.W. Advances in the Direct Strength Method of cold-formed steel design. Thin-Walled Structures 140: 533-541, 2019.

[27] Willis C.T., Wallace B. Behaviour of cold-formed steel purlins under gravity loading. Journal of Structural Engineering, 116(8): 206-2069, 1990.

[28] Yu C., Schafer B.W. Local buckling tests on cold-formed steel beams. Journal of Structural Engineering 129(12): 1596-1606, 2003.

[29] La Boube R.A. Simplified design approach for laterally braced purlins subjected to wind uplift. Proceedings of the 7th Int. Spec. Conf. on Cold-Formed Steel Structures, St. Louis, MO. November, 1984.

[30] Yang J., Liu Q. An experimental study into flexural behaviour of sigma purlins attached with roof sheets. Engineering Structures 45: 481-495, 2012.

[31] Nguyen V.B., Pham C.H., Cartwright B., English M.A. Design of new cold rolled purlins by experimental testing and Direct Strength Method. Thin-Walled Structures, 118, 105-112, 2017.

[32] Becque J., Rasmussen K.J.R. Stability of Z-section purlins used as temporary struts during construction. Journal of Structural Engineering 139(12), 04013009, 2013.

[33] Niu S., Rasmussen K.J.R., Fan F. Distortional-global interaction buckling of stainless steel C-beams: Part I – Experimental investigation. Journal of Constructional Steel Research 96, 127-139, 2014.

[34] Kyvelou P., Gardner L., Nethercot D.A. Testing and analysis of composite cold-formed steel and wood-based flooring systems. Journal of Structural Engineering 143(11), 1596-1606, 2017.

[35] Kyvelou P., Gardner L., Nethercot D.A. Finite element modelling of composite cold-formed steel flooring systems. Engineering Structures 158, 28-42, 2018.

[36] Almatrafi M., Theofanous M., Dirar S., Bock M. Structural response of cold-formed lipped Z purlins – Part 2: Numerical modelling and optimization of lip size. Thin-Walled Structures. (submitted).

[37] BS EN ISO 6892-1:2009. British Standard: Metallic Materials - Tensile Testing. Part 1: Method of Test at Ambient Temperature, The Standards Policy and Strategy Committee, 2009.

[38] Haidarali M. R., Nethercot D.A. Finite element modelling of cold-formed steel beams under local buckling or combined local/distortional buckling. Thin-Walled Structures, 49(12), 1554-1562, 2011.

[39] Shifferaw, Y., Schafer, B.W. Inelastic bending capacity of cold-formed steel members. Journal of Structural Engineering 138(4): 468-480, 2012.

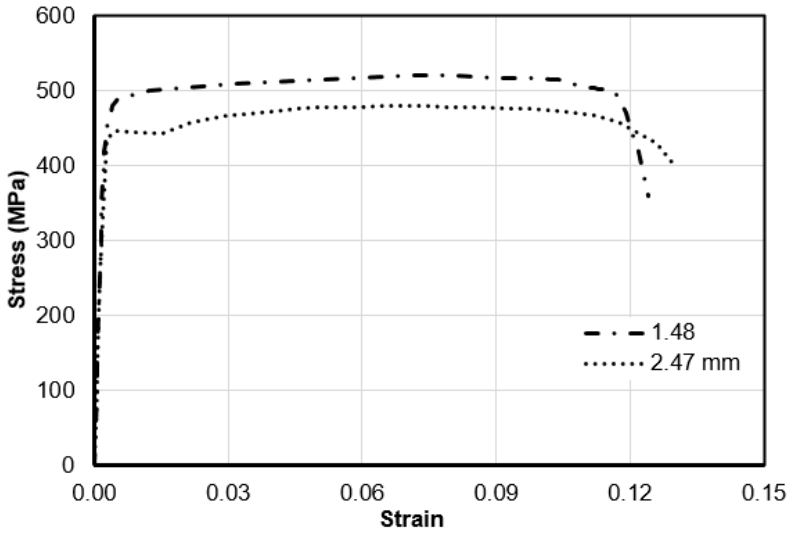

Fig.1: Typical stress-strain response of material coupons.

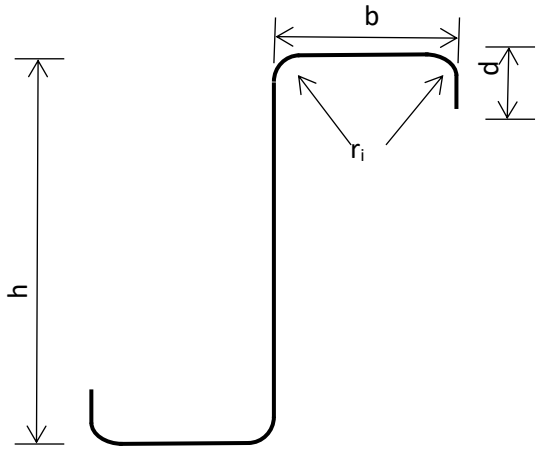

Fig. 2: Cross-section geometry and symbols.

Fig. 3: Typical angle strut and connection of strut and purlins.

Fig. 4: End detail over the support.

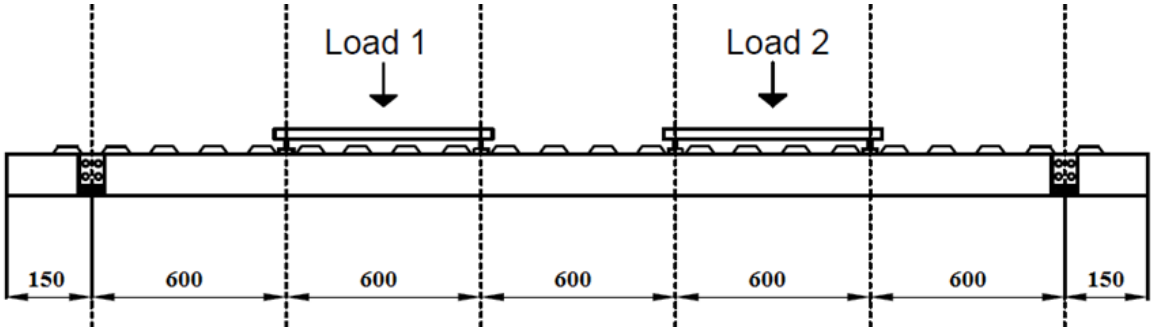

Fig. 5: Overview of test setup (dimensions in mm).

Fig. 6: Experimental setup prior to testing and employed instrumentation.

Fig. 7: Failure mode of Z14613 - interaction of distortional buckling with local buckling of the lip at mid-span.

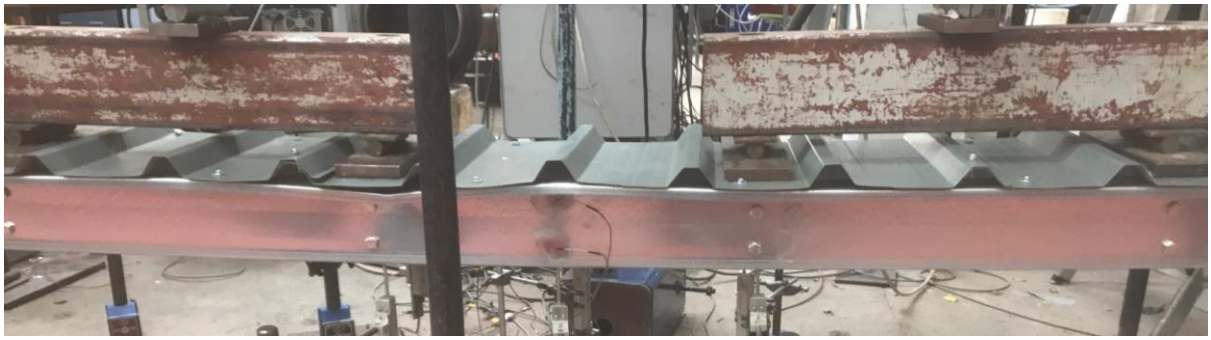

Fig. 8: Failure mode of Z14620 - distortional buckling.

Fig. 9: Failure mode of Z17613 - distortional buckling and interaction with local buckling of lip

Fig. 10: Failure mode of Z17625 - distortional buckling and interaction with local buckling of lip following material yielding.

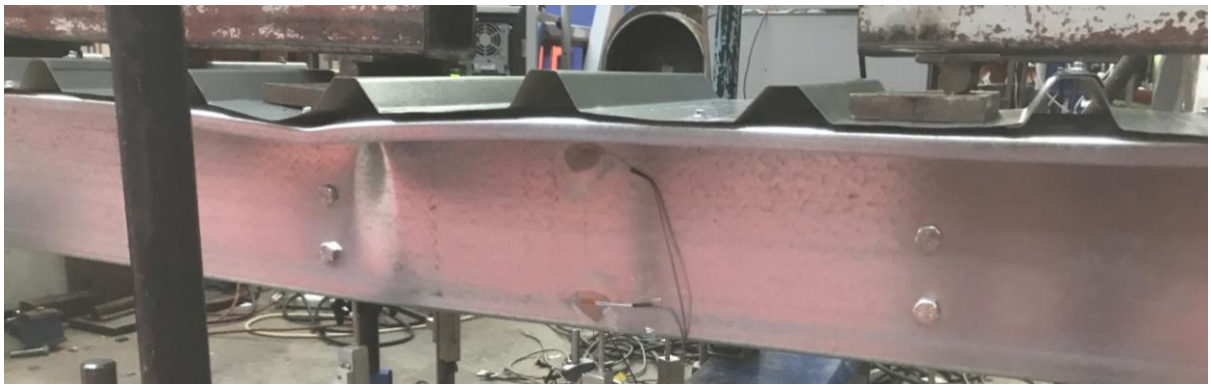

Fig.11: Failure mode of Z20620 - distortional buckling and web crippling after the peak load.

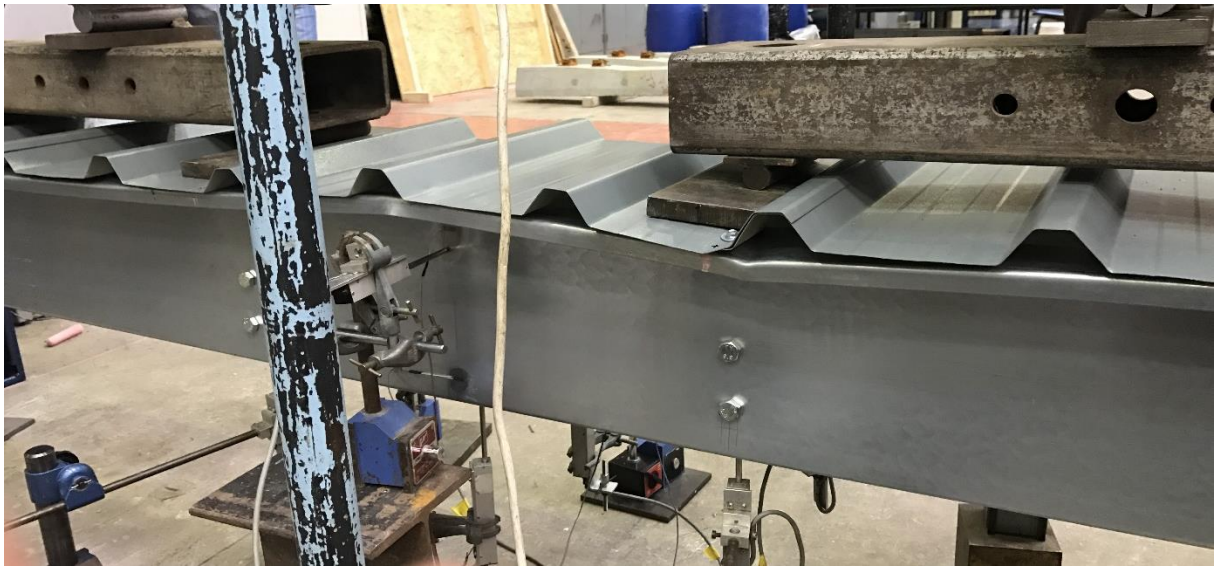

Fig.12: Failure mode of Z24615 - distortional buckling and interaction with local buckling of lip.

Fig.13: Failure mode of Z24620 - distortional buckling.

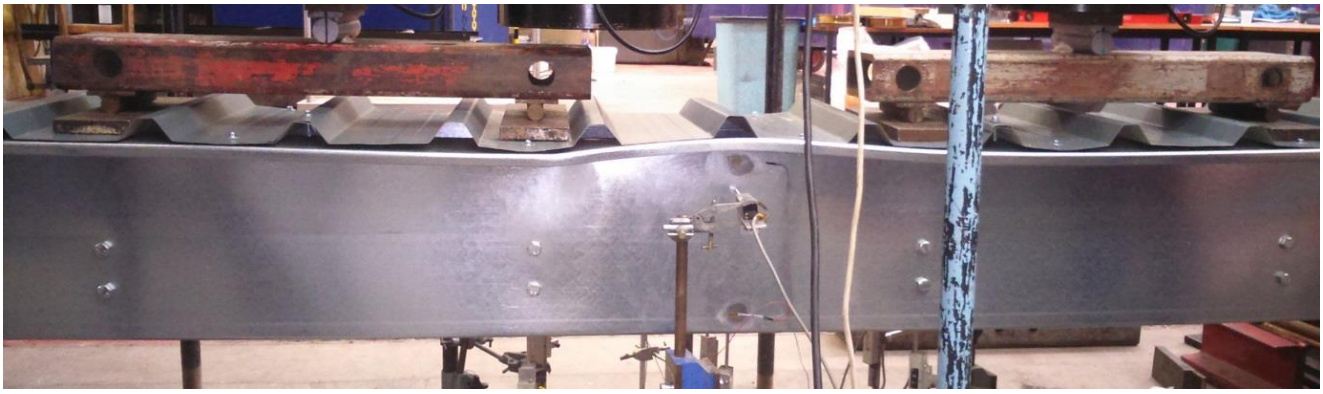

Fig.14: Failure mode of Z30718 - distortional buckling and localization of failure at left loading point (i.e. web crippling) after the peak load.

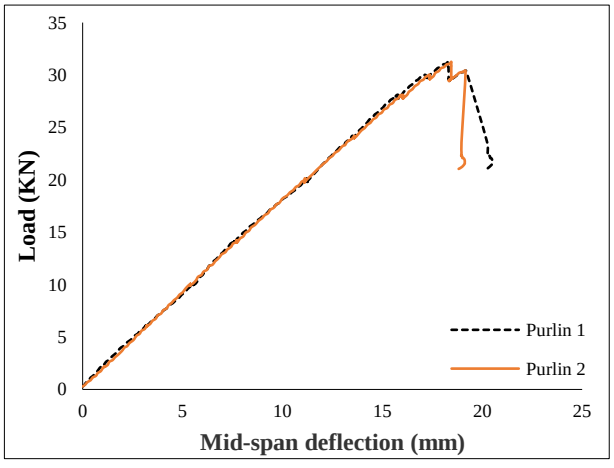

a) Z17613

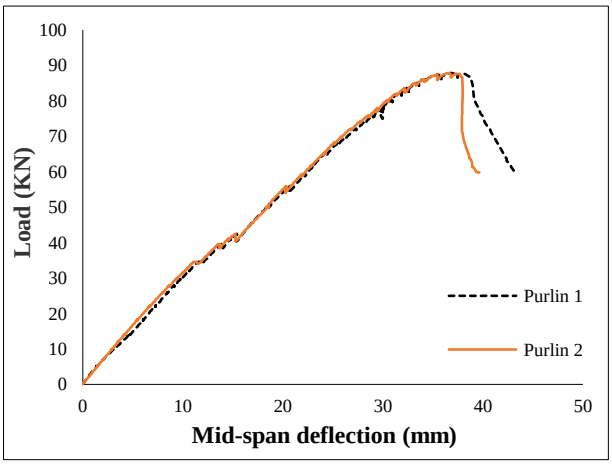

b) Z17625

Fig.15: Load - mid-span deflection response of specimens Z17613 and Z17625.

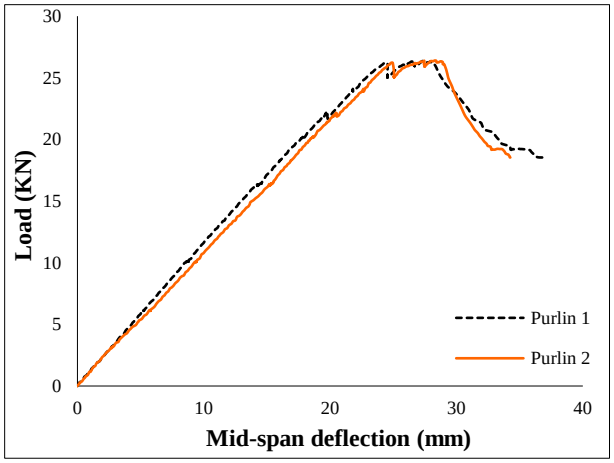

a) Z14613

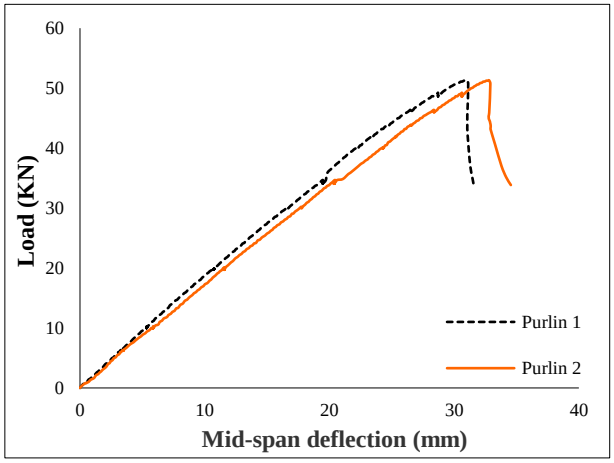

b) Z14620

Fig.16: Load - mid-span deflection response of specimens Z14613 and Z14620.

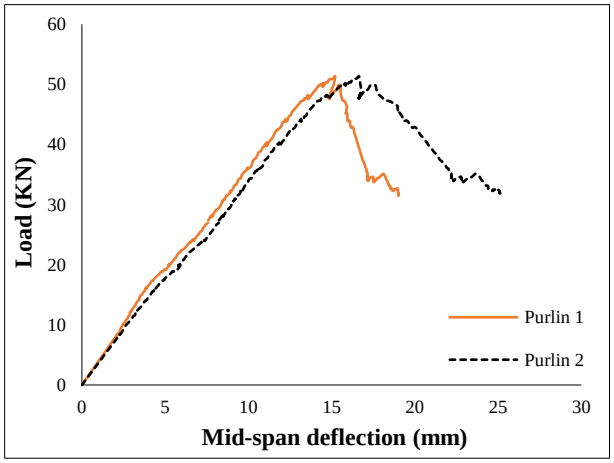

a) Z24615

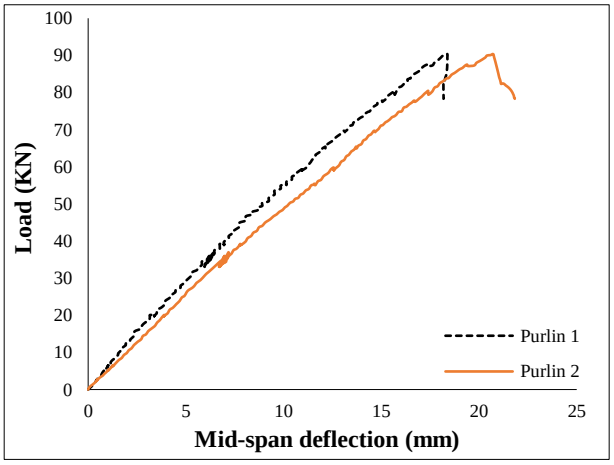

b) Z24620

Fig.17: Load - mid-span deflection response of specimens Z24615 and Z24620.

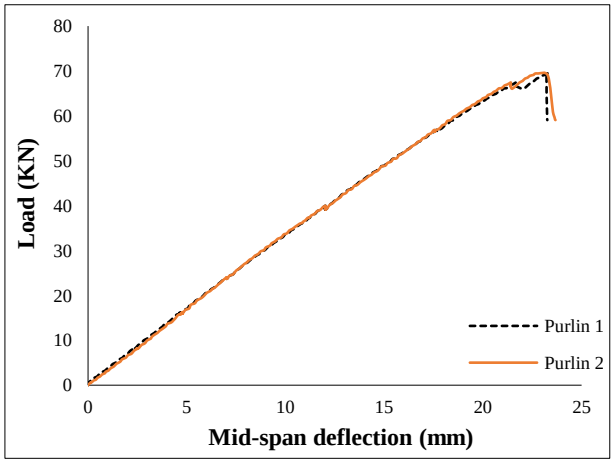

a) Z20620

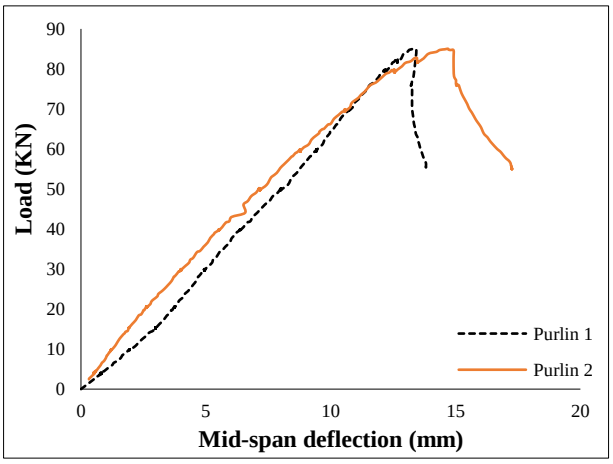

b) Z30718

Fig.18: Load - mid-span deflection response of specimens Z20620 and Z30718.

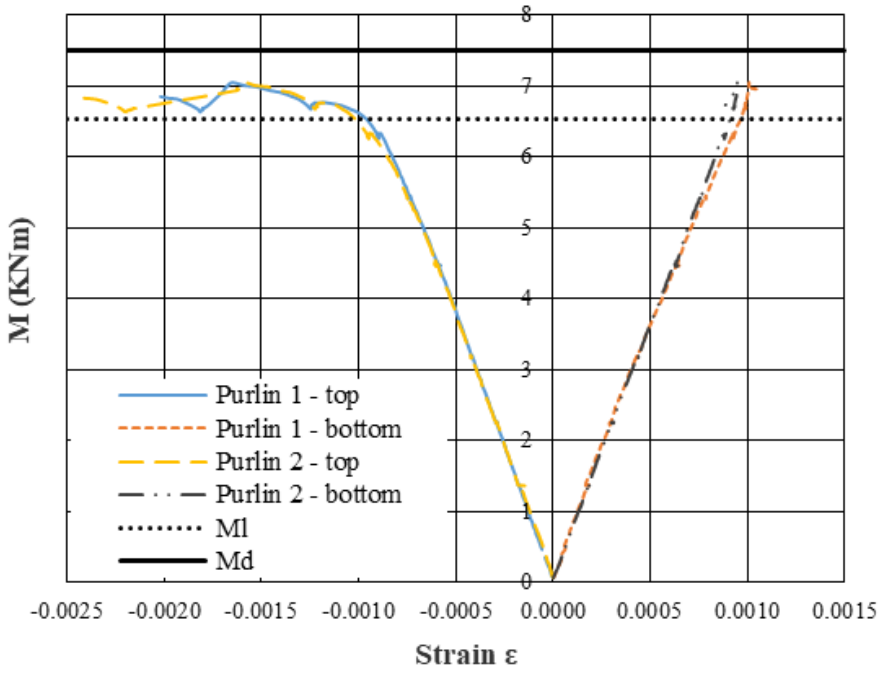

Fig.19: Moment-strain response of specimen Z17613

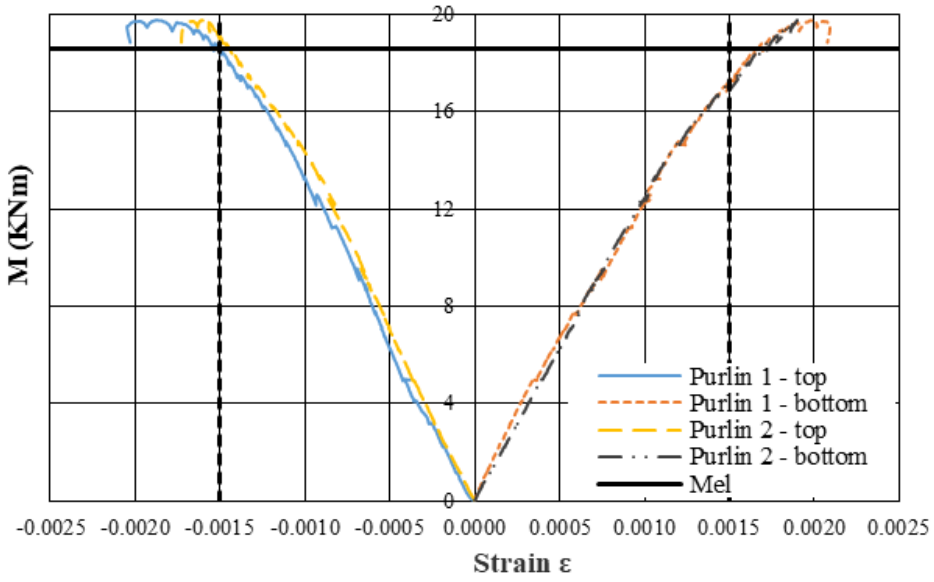

Fig.20: Moment-strain response of specimens Z17625

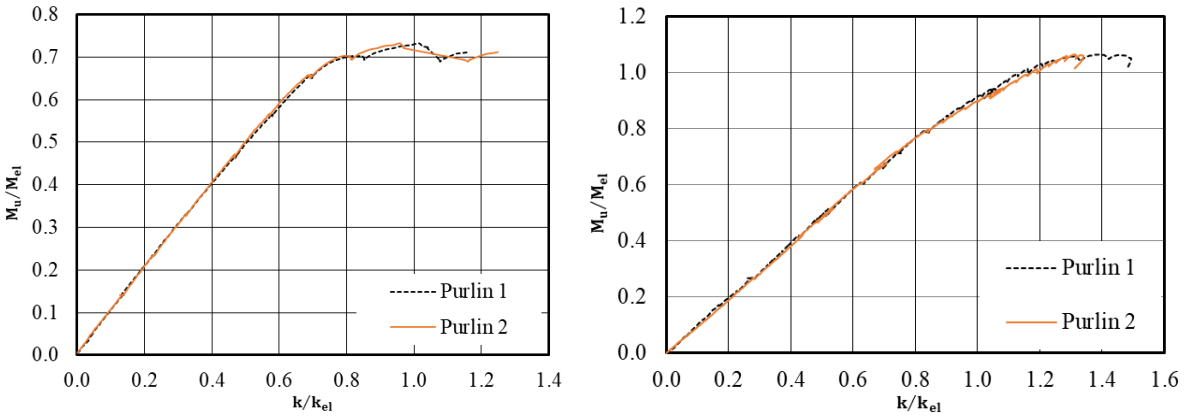

a) Z17613 b) Z17625

Fig.21: Moment - curvature response of Z17613 and Z17625

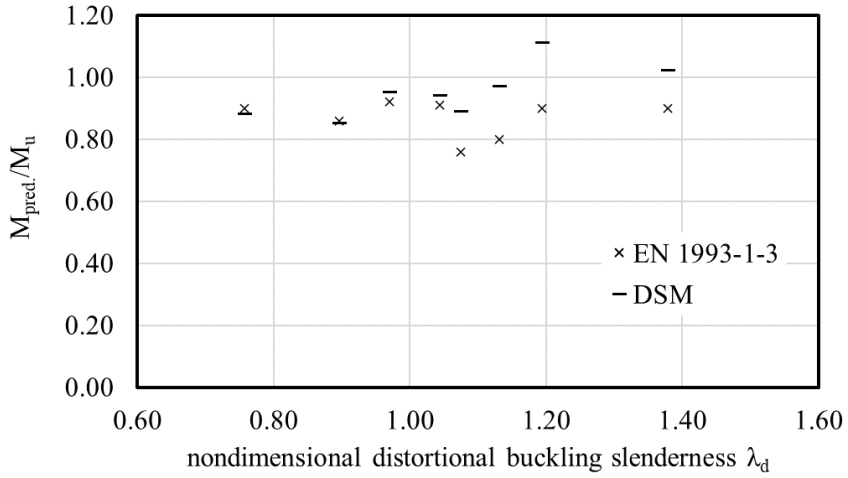

Fig. 22: Comparison of EN 1993-1-3 [10] and DSM [8] moment resistance predictions against test results

Table 1: Material properties from tensile coupon tests.

t (mm)	E (N/mm^2)	f_y (N/mm^2)	$f_{1.0}$ (N/mm^2)	f_u (N/mm^2)	ε_f (%)	material response
1.29	193000	447	470	480	14.7	rounded
1.48	212000	482	484	521	14.5	rounded
1.76	205000	476	481	522	14.0	rounded
1.96	199000	457	460	532	25.0	yield plateau
2.47	206000	461	470	517	24.0	yield plateau

Table 2: Measured geometric dimensions of tested specimens.

Section	h (mm)	b (mm)	d (mm)	t (mm)	ri (mm)
Z14613	145.41	61.37	18.61	1.28	4.31
Z14620	145.68	63.35	17.34	1.96	4.07
Z17613	176.75	61.71	19.51	1.29	3.84
Z17625	176.13	63.7	20.95	2.47	4.05
Z20620	200.00	66.4	19.64	1.95	4.44
Z24615	239.75	65.3	20.47	1.48	3.80
Z24620	243.83	66.35	19.5	2.00	4.00
Z30718	300.25	75.1	16.95	1.76	4.05

Table 3: Key experimental results and observed failure modes.

Section	M_u (kNm)	M_{el} (kNm)	M_u/M_{el}	$M_{cr,l}$ (kNm	$M_{cr,d}$ (kNm)	Observed failure mode
Z14613	5.94	7.15	0.83	6.3	6.19	D/L interaction
Z14620	11.54	11.63	0.99	23.21	14.46	D
Z17613	7.03	9.59	0.73	6.53	7.50	D/L interaction
Z17625	19.77	18.59	1.06	48.74	32.44	Yielding followed by D/L interaction
Z20620	15.62	18.55	0.84	23.22	19.73	D followed by WC
Z24615	11.55	18.76	0.62	9.78	13.16	D/L interaction
Z24620	20.33	25.27	0.80	22.96	23.20	D
Z30718	19.13	31.96	0.60	14.76	16.8	D followed by WC

Table 4: Assessment of design methods.

Section	M_u (kNm)	λ_d	λ_l	M_{EC3} (kNm)	M_{DSM} (kNm)	M_{EC3}/M_u	M_{DSM}/M_u
Z14613	5.94	1.07	1.07	4.51	5.29	0.76	0.89
Z14620	11.56	0.90	0.71	9.97	9.79	0.86	0.85
Z17613	7.04	1.13	1.21	5.63	6.83	0.80	0.97
Z17625	19.77	0.76	0.62	17.74	17.42	0.90	0.88
Z20620	15.62	0.97	0.89	14.40	14.79	0.92	0.95
Z24615	11.55	1.19	1.39	10.35	12.79	0.90	1.11
Z24620	20.33	1.04	1.05	18.41	19.11	0.91	0.94
Z30718	19.13	1.38	1.47	17.18	19.48	0.90	1.02
				Mean		0.87	0.95
				COV		0.07	0.09